Growth of Nd-doped YAG powder by sol spray process

**S. K. Durrani · K. Saeed · A. H. Qureshi ·
M. Ahmad · M. Arif · N. Hussain · T. Mohammad**

Abstract Yttrium aluminum garnet (YAG) and neo-
dymium-doped yttrium aluminum garnet (Nd-YAG) nano-
crystalline powders were successfully grown using cost
effective sol spray process without the addition of any
chelating agent or organic templates. Thermal decompo-
sition behavior was studied by thermogravimetry (TG) and
differential thermal analysis (DTA). Results revealed that
crystallization of YAG started around 920 °C. The
shrinkage/expansion behavior of synthesized powder was
examined by dilatometer and revealing that sintering
kinetics of these materials can be related to the evaporation
of binder and formation of crystalline phases. Nano-crys-
tallinity and garnet structure of YAG and Nd-YAG speci-
mens were analyzed by Raman, fourier transform infra red
(FTIR), and X-ray diffraction (XRD) techniques. XRD
patterns were indexed using Rietveld refinement method.
Smaller lattice parameter and a small change in atomic
position of oxygen were found in Nd-YAG when compared
with YAG structure. Scanning electron microscope (SEM)
results indicated that particle size of Nd-YAG was
<150 nm. The morphology of Nd-YAG nanosized powder
was rounded in shape.

S. K. Durrani · K. Saeed · A. H. Qureshi (✉) · M. Arif ·
N. Hussain
Materials Division, Directorate of Technology, PINSTECH, P.O.
Nilore, Islamabad, Pakistan
e-mail: ammadqureshi@yahoo.com; ammad@pinstech.org.pk

M. Ahmad
Physics Division, Directorate of Science, PINSTECH, P.O.
Nilore, Islamabad, Pakistan

T. Mohammad
Biophotonic Laboratory, NILOP, P.O. Nilore, Islamabad,
Pakistan

Introduction

The oxide system Y_2O_3–Al_2O_3 is promising material for
optical, electronic, and structural applications. These oxi-
des are attractive host materials for the development of
advanced phosphors with their general chemical stability
and resist saturation at high current excitation. The com-
pound $Y_3Al_5O_{12}$ commonly called an yttrium aluminum
garnet (YAG) adopts the cubic garnet structure. When this
is doped with a transition metal or lanthanide element, it
becomes an important material for solid state laser which is
widely used in luminescence systems, window materials
for a variety of lamps and for fiber-optics telecommuni-
cation systems [1–3]. Single crystal neodymium-doped
yttrium aluminum garnet Nd-$Y_3Al_5O_{12}$ (Nd-YAG) lasers
are extensively and widely utilized for various applications
in optical field and solid state lasers [4–6]. There are sev-
eral methods available in literature to produce YAG
nanopowder with good chemical, physical, and optical
characteristics. Such methods include conventional mixed
oxide [7], combustion method [8, 9], co-precipitation [10,
11], hydrothermal synthesis [12, 13], and sol gel method
[14, 15]. Recent investigations [16–18] indicated that sol
gel processes using metal alkoxides enable the preparation
of YAG phosphor ceramic materials with better physico-
chemical properties but it is not an economical process due
to high cost of precursors. However, sol spray process is an
area of recent research work for rapid and controlled syn-
thesis of homogeneous nano-sized powders which have
low sintering temperature, high density and improved
microstructure for the fabrication of ceramics [19]. In sol

spray process, the sol solutions are dehydrated directly into single phase nano-crystalline ceramic powders by spraying into a preheated temperature controlled Pyrex glass column by means of compressed air atomization without addition of any organic chelating agent or organic templates. Such process is likely to produce less agglomerated powders. In present study, the Nd-YAG oxide materials were prepared by sol spray process with an aim to determine the feasibility of process for the growth of nanosized YAG and Nd-YAG powders.

Experimental

Synthesis of powders

Highly pure neodymium oxide Nd_2O_3 (99.9% Merck), yttrium nitrate $Y(NO_3)_3 \cdot 6H_2O$ and aluminum nitrate $Al(NO_3)_3 \cdot 9H_2O$ (99.9% Fluka) were used as starting materials. Nitrate solutions with molar cationic ratio of Y:Al of 3:5 were prepared by dissolving the desired amount of $Y(NO_3)_3 \cdot 6H_2O$ and $Al(NO_3)_3 \cdot 9H_2O$ in CO_2-free distilled water and stirred for 2 h at room temperature. Aqueous solution of 1.1 at% neodymium was prepared by dissolving 1.28 g of Nd_2O_3 in minimum quantity of nitric acid and CO_2-free distilled water. After complete stirring, nitrate solutions were de-nitrated with anion exchange resin to get the desired sol. The sol was dehydrated directly into powder by spraying it into a preheated temperature controlled Pyrex glass column using compressed air atomization as described elsewhere [19]. The aqueous feed sol of sample was sprayed into upper end of vertical Pyrex glass column at a rate of 40 mL/h. The operating temperature of column was maintained at 155–165 °C. The powder was deposited on the inner walls of Pyrex glass column and finally the dried powder was collected in a glass collector placed at the lower open end of column using abrasive glass stick. Before grinding, some of the powder specimens of Nd-YAG (1.1 at.%) were first heated at 180 °C in static air oven, calcined at 600 °C for 5 h and then subjected to 900 °C for 12 h using box furnace. The calcined specimens were furnace-cooled and ground to fine powder.

Compaction and sintering

The oxide powder of Nd-YAG was used for pellet fabrication. The pellets were compacted using uniaxil hydraulic press of load capacity 10 ton/in² (1 ton/in² = 15.444 MPa). In order to obtain the crystalline Nd-YAG phase, the green pellets were sintered in tube furnace (static air) at 900, 1,100 and 1,600 °C for different durations (2–5 h).

Instrumentation

For TG/DTA analysis, the samples were heated at a constant rate of 10 °C/min to 1,000 °C using Netzsch STA-409 simultaneous thermal analyzer. Shrinkage/expansion behavior was observed by dilatometer (Netzsch, DIL, 409) with heating rate of 10 °C/min up to 1,100 °C in static air. Fourier transform infrared (FTIR) spectra were measured using a FTIR spectrophotometer (Nicolet 7600, Thermo-Fisher, USA). The powders were dispersed in KBr and were studied at room temperature. The garnet structure of YAG and Nd-YAG was characterized by Raman spectroscopy (RS). The Raman spectra were recorded on micro Raman spectrometer (MST-1000A, DongWoo Optron Co.). Crystallinity of YAG specimens was determined by X-ray diffraction on a Rigaku Geiger flux instrument using Cu K_α radiation. The specimens were scanned for 2θ range from 15 to 80° keeping a step-size of 0.05. For Rietveld refinement analysis, the Nd-YAG specimen was slow-scanned maintaining step-size of 0.02 for 5 s. Microstructural features of synthesized materials and sintered pellets were observed by scanning electron microscope (LEO 440I). The powder samples for SEM observation were prepared by ultrasonic dispersion of a small amount of sample in ethanol for 10 min. A drop of the solution was put onto aluminum stud, dried in air and then coated via gold sputtering. The elemental composition of the oxide materials was measured by electron probe micro-analyzer (EPMA) attached with SEM. The unit cell content was calculated according to the procedure [15, 20].

Results and discussion

Thermal decomposition of YAG and Nd-YAG powders

The representative TG/DTA thermograms of powder specimen Nd-YAG prepared by sol spray process is shown in Fig. 1. The TG curve shows an overall mass loss of approximately 30.26% which occurs up to ∼700 °C. This mass loss can be attributed to the evolution of water molecules and partial decomposition of carbonates. Above 700 °C there is almost no mass loss. Both exothermic and endothermic peaks were observed in DTA thermograms. The endothermic peak at 200 °C may be assigned to the removal of bound water. The DTA curve shows a small exothermic peak at ∼920 °C which may be related to crystallization and crystal growth of YAG [21, 22].

Shrinkage and expansion

Figure 2 displays the dilatometry curve of the YAG powder which was calcined at 600 °C. The curve shows the
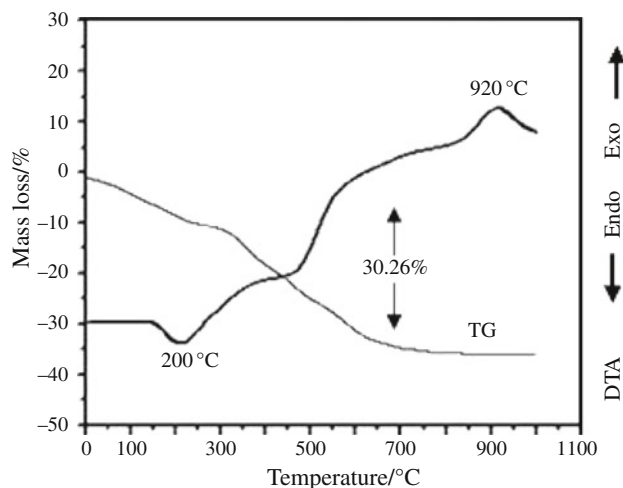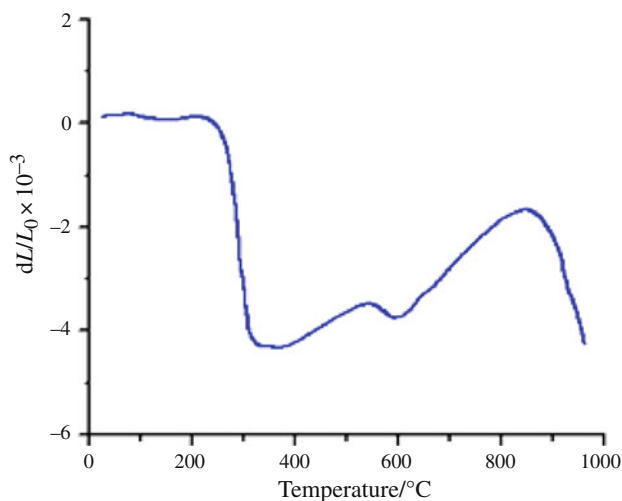
Fig. 1 TG/DTA curves of Nd-YAG powder

Fig. 2 Dilatometry curve of YAG powder

change in length during sintering of pressed pellets. There was no change in length on heating up to temperature of 275 °C. However, a large shrinkage occurred as a result of evolution of decomposed species between 300 and 400 °C. The temperature between 400 and 600 °C shows the expansion in the material. This expansion is due to the decomposition/expulsion of organic binder (PVA). Above 600 °C, there is gradual increase in dimensional changes (lattice parameters) which are due to the development of YAG phase. On the basis of dilatometry results, sintering was conducted between 900 and 1100 °C in order to obtain the full crystalline YAG phase.

FTIR and raman spectroscopy

Figure 3 presents FTIR spectrum of Nd-YAG powder calcined at 900 °C. There are strong metal oxygen vibrations at 793, 727, 686 cm^{-1} which are characteristics of
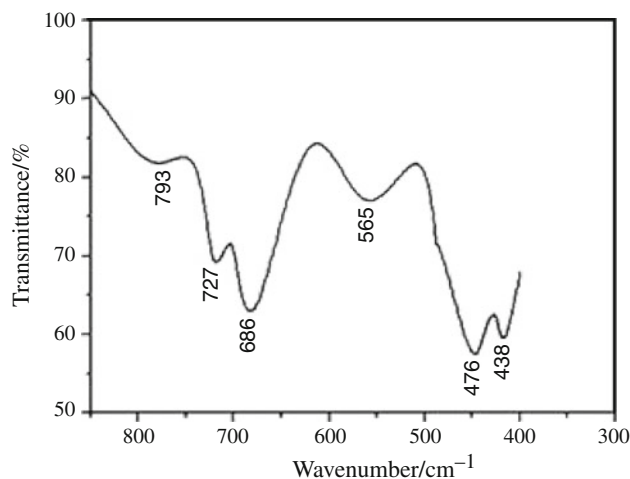

Fig. 3 FTIR spectra of Nd-YAG powder calcined at 900 °C

Y–O stretching vibrations band in tetrahedral arrangements. Absorption peaks at 565, 476, and 438 cm^{-1} are associated with stretching of Al–O bond in octahedral arrangements of garnet structure. The vibration modes for these bands are shown in Table 1. The peaks matched with the reported data of YAG [23, 24].
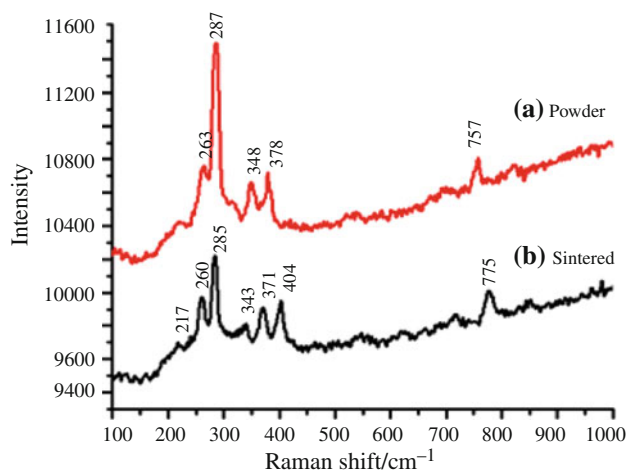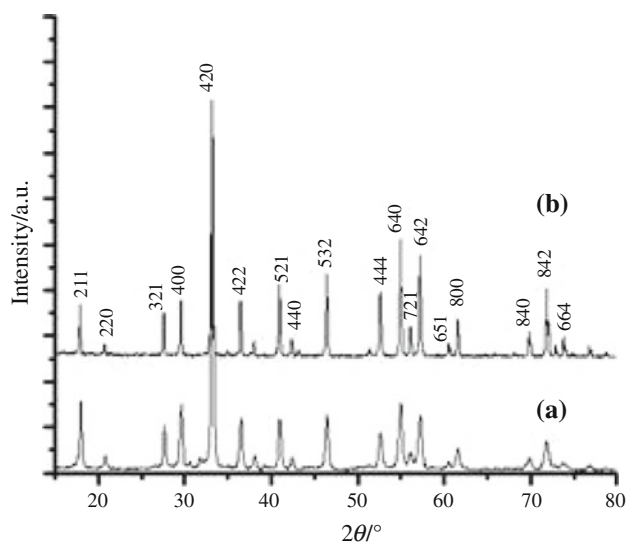
The Raman spectra of Nd-YAG (1.1 at.%) calcined at 900 °C and sintered at 1,100 °C for 2 h are presented in Fig. 4a, b. These spectra consisted of a series of bands located between 200 and 800 cm^{-1}. Both Raman absorption bands are similar, however, in case of sintered specimen, there is a slight shifting of peaks. The Raman band (Fig. 4b) at 775 cm^{-1}, bands with medium intensity located at 404 and 343 cm^{-1} and two weak intensity bands at 217 and 285 cm^{-1} are in good agreement with those reported in literature for bulk crystalline YAG [25]. The Raman bands around 540 and 691 cm^{-1} not observed in the spectra of Nd-YAG (1.1 at.%) are believed to have disappeared due to the multiple lattice distortions induced by the nano-crystalline character of the powders. The Nd^{3+} replaces the Y^{3+} of the Y–O dodecahedron in Nd-YAG crystal hence, new Raman peaks arise due to the symmetric bending vibration of the Nd–O bond. However, the Nd^{3+} concentration in present Nd-YAG crystal is only 1.1 at.% and therefore the intensity of Raman peaks is too weak to be observed.

Phase analysis and crystal structure

Figure 5a, b shows XRD pattern of the Nd-YAG powder calcined at 900 °C (Fig. 5a) and sintered at 1,600 °C (Fig. 5b) for 2 h in air. All peaks appearing in both diffractograms show single-phase crystalline Nd-Y$_3$Al$_5$O$_{12}$ with a well-pronounced garnet structure. However, crystallinity enhances after sintering at 1,600 °C. The main peak centers at $2\theta = 33.35°$ and corresponds to crystal

Table 1 FTIR analysis of Nd-Y$_3$Al$_5$O$_{12}$

Wave-numbers/cm^{-1}	Band assignment	Vibration mode
793	Y–O	Strong metal oxygen stretching vibrations band in tetrahedral arrangement
727	Y–O	Asymmetric stretching
686	Y–O	Symmetric stretching
565	Al–O	Stretching of vAl–O band in octahedral sites
476	Al–O	Scissor and symmetric stretching band
438	Al–O	Stretching band

Fig. 4 a, b Raman spectra of Nd-YAG (a) calcined at 900 °C and (b) sintered at 1,100 °C for 2 h

Fig. 5 a, b XRD patterns of Nd-YAG (a) calcined at 900 °C and (b) sintered at 1,600 °C

plane with Miller indices of 420, which is characteristic of YAG [23]. The sharp peaks in XRD patterns may be ascribed to cubic Y$_3$Al$_5$O$_{12}$. The XRD peaks were indexed in terms of garnet structure according to standard JCPDS 33-0040.

In order to obtain structural parameters, the Rietveld refinement method [26, 27] was performed for Y$_3$Al$_5$O$_{12}$ and Nd-Y$_3$Al$_5$O$_{12}$. Figure 6 shows the Rietveld refinement XRD pattern of Nd-YAG. The Y$_3$Al$_5$O$_{12}$ crystallizes in a body centered cubic structure, space group la–3d, lattice parameter $a = 12.023$ Å and Wyckoff position: Y at 24c (0.125, 0, 0.25), Al (1) at 16a (0, 0, 0), Al (2) at 24d (0.375, 0, 0.25) and O at 96h ($x = -0.04$, $y = 0.055$, $z = 0.14$). After refinement, the lattice parameters of Y$_3$Al$_5$O$_{12}$ $a = 12.024(4)$ Å and oxygen position $x = -0.02944$, $y = 0.04492$, $z = 0.1325$ were found. The reliability factors of $R_p = 10.00\%$, $R_{wp} = 13.72\%$, $R_{exp} = 6.48\%$, and $X^2 = 4.47$ were achieved. Cell parameters and cell volume were calculated by least square Rietveld method and found to be 12.024 Å and 1738.56 (Å)^3 for the Nd-YAG, indicating partial substitution of Y^{3+} sites with Nd^{3+} cations, Tables 2 and 3. The cell parameters were comparable with reported values of YAG (cubic) crystals [28]. It was observed that sol spray process provided well-developed Nd-YAG at low temperature 900 °C. There are no diffraction trace peaks of dopant oxide (Nd$_2$O$_3$) in XRD pattern. The formation of single phase YAG with a homogeneous distribution of dopant at 900 °C suggested that this synthesis temperature is rather low for such kinds of ceramics. The average size of nano-crystallites was determined from the broad diffraction lines of X-ray patterns according to Scherrer's formula [29]. The grain size of YAG sintered at 900 °C is about 150 nm. The *average* increases with the increase of sintering temperature. When sintered at 1,100 °C, the grain size was found quite uniform, with an average grain size of about 200 nm.

Microstructure and micro analysis

Figure 7a–c exhibits SEM images of powder specimen of YAG (Y$_{2.97}$Al$_{5.03}$O$_{11.85}$) calcined at 900 °C for 4 h (Fig. 7a), pellet specimen of YAG sintered at 1,100 °C for 2 h (Fig. 7b), and pellet specimen of Nd-YAG sintered at 1,100 °C for 2 h (Fig. 7c). Figure 7a revealed that the powder specimen of YAG has an average grain size of about 0.2 μm (200 nm), whereas a much higher grain size of 5 μm resulted from pellet specimen sintered at 1,100 °C for 2 h (Fig. 7b). Figure 7c revealed that the morphology of sintered specimen of Nd-YAG had somewhat rounded in shape with grain size of <0.15 μm (<150 nm). It is thought that Nd has inhibited the grain growth of YAG during
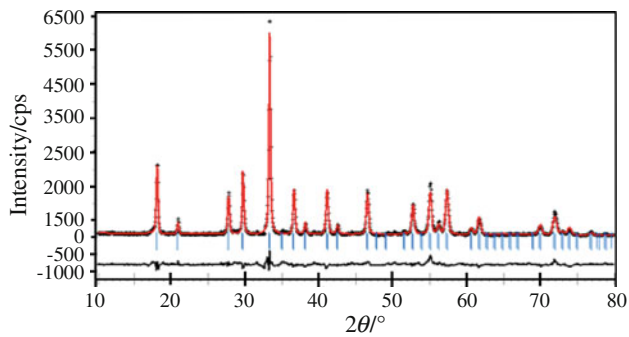
Fig. 6 Refined X-ray diffraction for Nd-YAG observed (+), and calculated (−). Bottom curve shows appreciable matching between observed and calculated pattern. The reflection positions are also marked

Table 3 Refined positional parameters obtained from the Rietveld refinement of $Y_3Al_5O_{12}$ X-ray diffraction data

Atoms	Positions	x	y	z	B
Y	24c	0.1250	0.0000	0.2500	0.6000
Al(1)	16a	0.0000	0.0000	0.0000	0.5000
Al(2)	24d	0.3750	0.0000	0.2500	0.3000
O	96h	−0.02944	0.04492	0.1325	6.6000

Lattice parameter/Å	Unit cell volume/Å^3	R_p/%	R_{wp}/%	R_{exp}/%	GOF/%
12.024	1738.56	10.00	13.72	6.48	4.47

Table 2 X-ray diffraction data of $Y_3Al_5O_{12}$

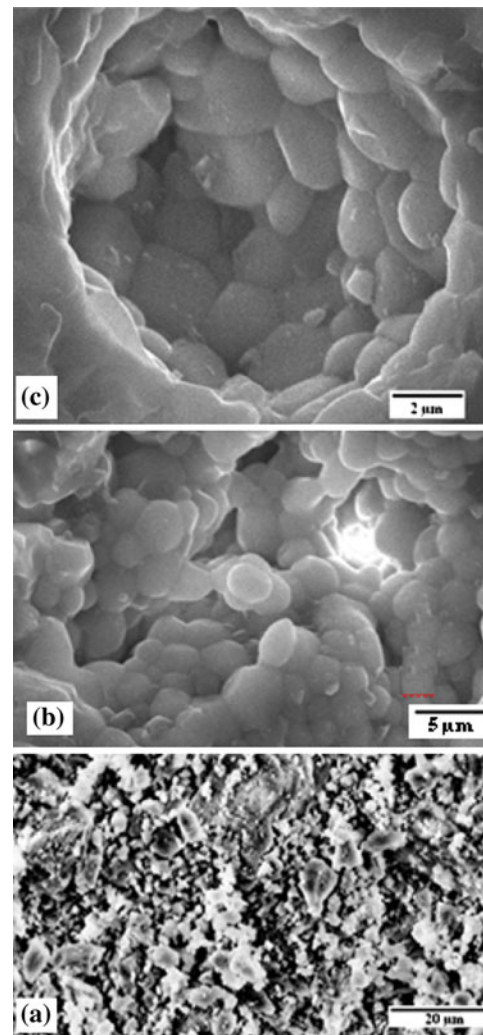| Intensity $(I/I°)$/%	d spacing/Å	Miller indices			Identification of phases
		h	k	l	
30	4.924	2	1	1	$Y_3Al_5O_{12}$
7	4.259	2	2	0	
19	3.225	3	2	1	$Y_3Al_5O_{12}$
28	3.016	4	0	0	$Y_3Al_5O_{12}$
100	2.696	4	2	0	$Y_3Al_5O_{12}$
22	2.456	4	2	2	$Y_3Al_5O_{12}$
7	2.365	4	3	1	
22	2.201	5	2	1	$Y_3Al_5O_{12}$
6	2.129	4	4	0	
24	1.955	5	3	2	$Y_3Al_5O_{12}$
17	1.737	4	4	4	
29	1.669	6	4	0	$Y_3Al_5O_{12}$
8	1.636	7	21	1	
23	1.607	6	4	2	$Y_3Al_5O_{12}$
10	1.506	8	0	0	
12	1.345	8	4	0	
28	1.315	8	4	2	$Y_3Al_5O_{12}$
4	1.281	6	6	4	
System	Cubic				
Symmetry	1a–3d				
Unit cell parameter	12.024 Å				
Unit cell volume	1738.56 (Å)^3				

Fig. 7 a–c SEM images. **a** YAG powder calcined at 900 °C for 4 h, **b** YAG pellet sintered at 1,100 °C for 2 h, and **c** Nd-YAG pellet sintered at 1,100 °C for 2 h

sintering, so the grain size has reduced as compared to YAG sintered under the same conditions.

Figure 8 shows the EPMA spectrum of Nd-YAG specimen sintered at 1,100 °C (SEM, Fig. 7c). The unit cell formula was estimated using oxide formula method [20] and the data are presented in Table 4. The result uncovered that YAG specimen consisted of single $Y_{3.04}Al_{4.96}O_{12}$ phase with atomic ratio of yttrium, aluminum, and oxygen close to 3:5:12. Thus, the $Y_{3.04}Al_{4.96}O_{12}$ and $Nd_{0.10}Y_{2.96}Al_{4.93}O_{12}$ oxide powders with nearly single cubic phase were obtained.
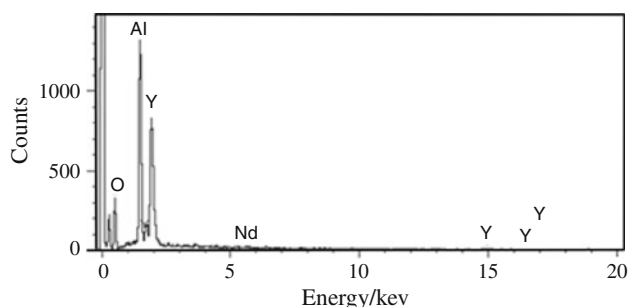
Fig. 8 EPMA spectra of Nd-YAG

Table 4 Determination number of atoms per unit cell

Elements	Composition		Mole ratios	No. of atoms per unit cell
	Atomic %	Oxides %		
Aluminum (Al)	8.46	25.04	0.2455	4.93
Yttrium(Y)	57.15	30.30	0.1474	2.96
Neodymium (Nd)	0.92	1.74	0.005	0.10
Oxygen	Calculated from empirical formula [15]			12
Unit cell formula	$Y_{3.04}Al_{4.96}O_{12}$			$Nd_{0.10}Y_{2.96}Al_{4.93}O_{12}$

Conclusions

The fine and homogeneous crystals of $Y_3Al_5O_{12}$ and Nd-$Y_3Al_5O_{12}$ oxide powder have successfully been grown by sol spray pyrolysis process without using organic templates. FTIR spectrum of crystals grown at 900 °C unfolded the presence of Al–O and Y–O bands. The presence of compact water molecule was detected. The results of Raman spectra indicated that the undoped YAG and Nd-YAG crystals had similar spectra and doping did not influence the spectral properties such as lattice vibration. The XRD and SEM studies confirmed that the sol spray pyrolysis process produced single-phase garnet structure of $Y_{3.04}Al_{4.96}O_{12}$ and $Nd_{0.10}Y_{2.96}Al_{4.93}O_{12}$ powder. The synthesized products had composition uniformity, lower residual oxide, cubic phase with a ratio of yttrium, aluminum, and oxygen close to 3:5:12 ($Y_{2.97}Al_{5.03}O_{11.85}$) and smaller particle size. Single-phase $Y_{3.04}Al_{4.96}O_{12}$ and $Nd_{0.10}Y_{2.96}Al_{4.93}O_{12}$ powders with grain size ($\sim$10–15 μm) were obtained from the pellet specimen sintered at 1,100 °C for 2 h.

References

1. Caponetti E, Martino DC, Saladino ML. Preparation of Nd:YAG nanopowder in a confined environment. Langmuir. 2007;23: 3947–52.
2. Lu J, Ueda K, Yagi H, Yanagitani T, Akiyama Y, Kaminskii A. Neodymium doped yttrium aluminium garnet ($Y_3Al_5O_{12}$) nanocrystalline ceramics: a new generation of solid-state laser and optical materials. J Alloys Compd. 2002;341:220–5.
3. Pakutinskiene I, Mathur S, Shen H, Kudabiene G, Jasaitis D, Kareiva A. From precursors to ceramic materials. II. Synthesis and specific features of new garnet structure compounds. Mater Sci (Medziagotyra). 2003;9:374–6.
4. Hreniak D, Strek W, Mazur P. Preparation, spectroscopy and morphology of Nd-YAG nanostructures. Mater Sci. 2002;20: 39–45.
5. Ikesue A. Polycrystalline Nd-YAG ceramics laser. Opt Mater. 2002;19:183–7.
6. Mah T-I, Parthasarthy TA, Lee HD. Polycrystalline YAG structural or functional. J Ceram Proc Res. 2004;5:369–72.
7. Naglieri V, Palmero P, Montanaro L. Preparation and characterization of alumina-doped powders for the design of multi-phasic nano-microcomposites. J Therm Anal Calorim. 2009;97: 231–7.
8. Costa AL, Esposito L, Medri V, Bellosi A. Synthesis of Nd-YAG material by citrate-nitrate sol-gel combustion route. Adv Eng Mater. 2007;9:307–12.
9. Guo X, Devi PS, Ravi BG, Parise JB, Sampath S, Hanson JC. Phase evolution of yttrium–aluminium–garnet (YAG) in a citrate–nitrate gel combustion process. J Mater Chem. 2004;14: 1288–92.
10. Li X, Li Q, Wang J, Yang S, Liu H. Synthesis of Nd^{3+} doped nano-crystalline yttrium aluminum garnet (YAG) powders leading to transparent ceramic. Opt Mater. 2007;29:528–31.
11. Caponeti E, Saladino ML, Serra F, Enzo S. Co-precipitation synthesis of Nd-YAG nano-powders: the effect of Nd dopant addition with thermal treatment. J Mater Sci. 2007;42:4418–27.
12. Hakuta Y, Seino K, Ura H, Adschiri T, Takizawa H, Arai K. Production of phosphor (YAG:Tb) fine particles by hydrothermal synthesis in supercritical water. J Mater Chem. 1999;9:2671–4.
13. Takamori T, David LD. Controlled nucleation for hydrothermal growth of YAG powders. J Am Ceram Soc Bull. 1986;65: 1282–6.
14. Devi PS, Li Y, Margolis J, Parise JB, Sampath S, Herman H, Hanson JC. Comparison of citrate-nitrate gel combustion and precursor plasma spray processes for the synthesis of yttrium aluminum garnet. J Mater Res. 2002;17:2846–51.
15. Chung BJ, Park JY, Sim SM. Synthesis of yttrium aluminum garnet powder by a citrate gel method. J Ceram Proc Res. 2003;4:145–50.
16. Vaqueiro P, Lopequea MA. Influence of complexing agents and pH on yttrium–iron garnet synthesized by the sol–gel method. Chem Mater. 1997;9:2836–41.
17. Tachiwaki T, Yoshinaka M. Novel synthesis of $Y_3Al_5O_{12}$ (YAG) leading to transparent ceramics. Solid State Commun. 2001;119: 603–6.
18. De La Rosa E, Diaz-Torres LA, Salas P, Arredondo A, Montoya JA, Angeles C, Rodriguez RA. Low temperature synthesis and structural characterization of nanocrystalline YAG prepared by a modified sol-gel method. Opt Mater. 2005;27:1793–9.
19. Durrani SK, Qureshi AH, Qayyum S, Arif M. Development of superconducting phases in BSCCO and Ba-BSCCO by sol spray process. J Therm Anal Calorim. 2009;95:87–91.
20. Thompson JS. A simple rhyme for a simple formula. J Chem Educ. 1988;65:704–5.

21. Cinibulk MK. Synthesis of yttrium aluminum garnet from a mixed-metal citrate precursor. J Am Ceram Soc. 2000;83: 1276–8.

22. Wang S, Xu Y, Lu P, Xu C, Cao W. Synthesis of yttrium aluminium garnet (YAG) from an ethylenediaminetetraacetic acid precursor. Mater Sci Eng B. 2006;127:203–6.

23. Vaidhyanathan B, Binner JGP. Microwave assisted synthesis of nanocrystalline YAG. J Mater Sci. 2006;41:5954–7.

24. Panneer SM, Subanna GN, Rao KJ. Translucent yttrium aluminum garnet: microwave-assisted route to synthesis and processing. J Mater Res. 2001;16:2773–6.

25. Chen YF, Lim PK, Lim S, Yang YJ, Hu LJ, Chiang HP, Tse WS. Raman scattering investigation of Yb:YAG crystals grown by the Czochralski method. J Raman Spectrosc. 2003;34:882–5.

26. Anderson MT, Poeppelmeier KR. Lanthanum copper tin oxide (La_2CuSnO_6): a new perovskite-related compound with an unusual arrangement of B cations. Chem Mater. 1991;3:476–82.

27. Young RA, editor. The Rietveld methods. Oxford: IUCR-Oxford University Press; 1995.

28. Kaithwas N, Deshmukh M, Kar S, Dave M, Lalla NP, Ryuh KS, Bartwal S. Preparation of $Y_3Al_5O_{12}$ nanocrystals by low temperature glycol route. Cryst Res Technol. 2007;42:991–4.

29. Culity BD, Stock SR. Elements of X-Ray diffraction. 2nd ed. Reading: Addition-Wesley; 1978.